catalysts

MDPI

Article

Naturally Nano: Magnetically Separable Nanocomposites from Natural Resources for Advanced Catalytic Applications

Rick A. D. Arancon [1], Zeid A. Al Othman [2], Thomas Len [1], Kaimin Shih [3], Leonid Voskressensky [4] and Rafael Luque [1,2,*]

[1] Departamento de Quimica Organica, Universidad de Cordoba, Campus de Rabanales, Edificio Marie Curie (C-3), Ctra Nnal IV-A, Km 396, E14014 Cordoba, Spain
[2] Department of Chemistry, College of Science, King Saud University, P.O. Box 2455, Riyadh 11451, Saudi Arabia
[3] Department of Civil Engineering, The University of Hong, Haking Wong Building, Pokfulam Road, Hong Kong HK 852, China
[4] Faculty of Sciences, Peoples Friendship University of Russia (RUDN University), 6 Miklukho Maklaya str., Moscow 117198, Russia
* Correspondence: rafael.luque@uco.es

Abstract: The present manuscript describes the use of silk cocoons as a structuring agent for the formation of an iron-based active phase for the controlled oxidation of benzyl alcohol. Different samples were prepared using different calcination temperatures. X-ray diffraction and transmission electron microscopy showed a higher proportion of alpha-Fe_2O_3 phase and a higher global crystallinity at superior calcination temperature. In terms of catalytic activity, the sample treated at 500 °C presented the highest conversion reaching 47%, with selectivity in benzaldehyde of 75.9%.

Keywords: nanomaterials; silk cocoons; oxidation; Fe

Citation: Arancon, R.A.D.; Al Othman, Z.A.; Len, T.; Shih, K.; Voskressensky, L.; Luque, R. Naturally Nano: Magnetically Separable Nanocomposites from Natural Resources for Advanced Catalytic Applications. *Catalysts* **2022**, *12*, 1337. https://doi.org/10.3390/catal12111337

Academic Editors: Victorio Cadierno and Raffaella Mancuso

Received: 26 September 2022
Accepted: 19 October 2022
Published: 1 November 2022

Publisher's Note: MDPI stays neutral with regard to jurisdictional claims in published maps and institutional affiliations.

Copyright: © 2022 by the authors. Licensee MDPI, Basel, Switzerland. This article is an open access article distributed under the terms and conditions of the Creative Commons Attribution (CC BY) license (https://creativecommons.org/licenses/by/4.0/).

1. Introduction

The selective oxidation of alcohol in their corresponding aldehydes and ketones is a key step for oxidation reactions [1]. Benzaldehyde is industrially produced from the reaction of toluene and chromyl chloride during the Etard reaction [2]. However, the contamination by chlorine limits the valorization of the synthesized benzaldehyde. Thus, benzaldehyde production from benzyl alcohol oxidation was extensively studied since benzaldehyde is a commonly used platform molecule in fine chemical production [3]. This reaction could be performed using two main types of oxidant. On the one hand, the utilization of metal oxides such as chromates [4,5] or permanganates [6,7] could lead to pollution by heavy metals in the desired product. Moreover, this process does not respect the principle of green chemistry since a really low atom efficiency is obtained, and a large quantity of waste is generated. On the other hand, peroxide-like compounds are frequently reported for this reaction. The main ones include simple hydrogen peroxide as well as t-butylhydroperoxide [8,9]. However, as every application needs these compounds, issues related to their low stability during transportation and storage can be present.

In addition to a source of oxygen, a catalyst is often used in order to increase the reaction rate. Firstly, homogeneous systems were designed to reach high product yields [10,11]. However, recurrent problems of homogeneous catalyses, such as catalyst separation and recyclability, also apply here. To overcome these limitations; high interest has been put in developing heterogeneous counterparts. Catalysts based on supported noble metal nanoparticles are well known to be effective in a large number of applications [12–14] and were described as interesting for this oxidation reaction. Platinum [15,16], palladium, ruthenium [17,18], and gold [19,20] nanoparticles are most commonly used in com-

bination with both molecular oxygen or hydrogen peroxide. Among these metals, palladium-based material attracted particular interest due to their high activity and selectivity, in particular to the aldehyde product with respect to the carboxylic acid compound [21]. Thus, despite their higher prices, it represents a relevant alternative to Pt-based catalysts. A common strategy to improve the performance of Pd-based catalysts is the addition of another metal to design bimetallic particles. The most suitable candidate for this role appears to be gold. In Pd-Au bimetallic systems, modulation of catalytic activity, selectivity and stability became possible [22–24]. However, this noble metal-based catalyst suffers from a high cost and high risk of scarcity in the coming years, particularly with prospects at industrial scale [25].

The use of non-noble, non-expensive, non-toxic, and widely available metals can provide a more sustainable alternative. Iron can potentially be a perfect candidate, according to this description. In combination with hydrogen peroxide under mild batch reaction conditions, iron oxide nanoparticles were reported as highly active for the oxidation of different compounds, including alcohols, alkenes, or sulfides [26–31]. Supported by MCM-41, aluminosilicate, MIL-101, or Al-SBA-15, iron nanoparticles reached high performance in different alcohol oxidations. However, unsupported iron nanoparticles possess certain limitations. It was shown by both theoretical and experimental methods that the modification of iron oxide nanoparticles by epichlorohydrin can lead to higher performance [32]. It was ascribed to a promoted adsorption and decomposition of hydrogen peroxide. Thus, in the case of unsupported catalysts, a strategy is needed to optimize the performance of the iron active phase.

In 2019, 679,306 tonnes of silk cocoons were produced worldwide. That represented an increase of 15.9% in the last decade. The producers' podium is composed of China, India, and Thailand, with 410,000, 170,000, and 55,000 tonnes, respectively [33]. For five millennia, silk fibers produced by *Bomby Mori* were used in the textile industry. The development of this industry led to important cultural exchange throughout the silk route. This biocompatible fiber developed interesting porosity that could be useful in material science.

This paper used the natural nano-porosity of silk cocoons to design iron oxide nanoparticles. The catalytic materials were prepared by a mechanochemical ball-milling method. The resulting catalysts were employed in the oxidation of benzyl alcohol assisted by microwave irradiation.

2. Results and Discussion

XRD analyzed the prepared samples after calcination at 100 °C, 200 °C, and 300 °C. The results are exposed in Figure 1. The original sample is composed of only one phase, the magnetite Fe_3O_4. In this sample, only 21 wt% are in the crystalline phase, while the other 79 wt% are amorphous. The crystallite size was measured at 4 nm. The 100 °C sample appears almost completely amorphous since no diffraction peaks were detected. Thus, 100 °C appears as a high enough calcination temperature to completely destabilize the magnetite phase. Increasing the calcination temperature leads to higher crystallinity in the material. More precisely, both alpha-Fe_2O_3 and gamma-Fe_2O_3 are present after thermal treatment at 200 °C and 300 °C. For the 200 °C samples, the amount of alpha-Fe_2O_3, gamma-Fe_2O_3, and amorphous is 35 wt%, 21 wt%, and 44 wt%, respectively. In this sample, the crystal size of the alpha-Fe_2O_3 phase was about 26 nm, and 6 nm for gamma-Fe_2O_3. A higher crystallinity is obtained after calcination at 300 °C with an amount of alpha-Fe_2O_3, gamma-Fe_2O_3, and amorphous of 45 wt%, 27 wt%, and 28 wt%, respectively. Here, the crystal size of the alpha-Fe_2O_3 phase was about 26 nm, and 9 nm was for gamma-Fe_2O_3. Thus, a slightly larger crystallite size of gamma-Fe_2O_3 was measured after treatment at 300 °C.

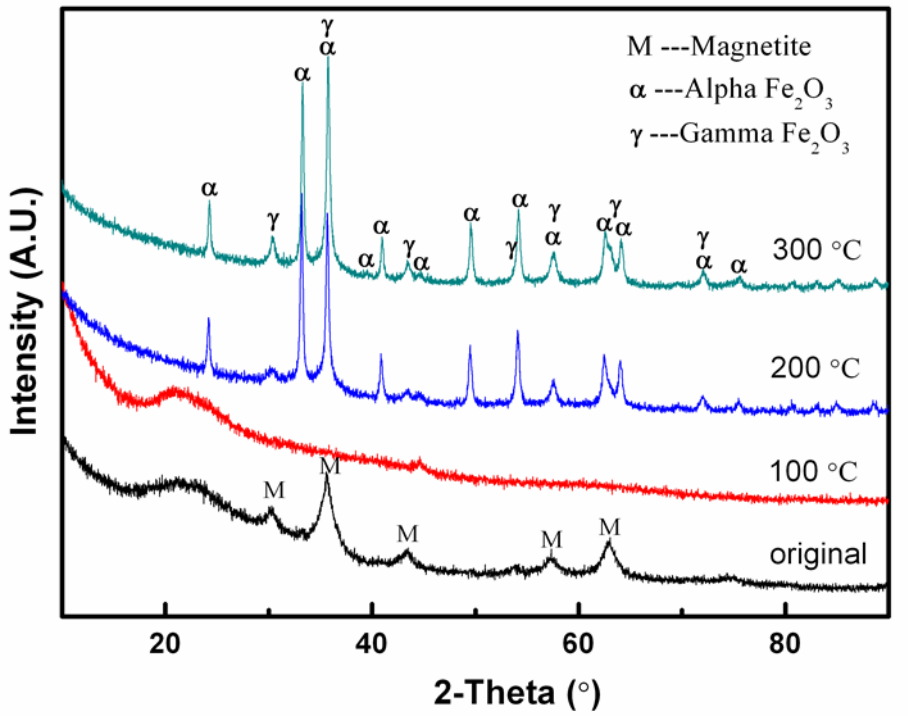

Figure 1. X-ray diffractograms of the original sample and samples calcined at 100 °C, 200 °C, and 300 °C.

Micrographs of these three materials obtained by transmission electron microscopy are compiled in Figure 2. Figure 2A,B represents the structure of the samples calcined at 100 °C and 200 °C, respectively. With these two images, onion-like lamellar structures clearly appear. However, low-defined structures are obtained due to low crystallinity. As previously seen by XRD, increasing the calcination temperature leads to higher material crystallinity. Figure 2C,D brings to light the well-defined onion-like structure of the sample calcined at 300 °C. On these micrographs, circular lamellar iron structures are observed. In accordance with XRD, the 300 °C sample seems to be more precisely defined with higher phase homogeneity. Without the use of silk cocoon as a sacrificial structural agent, synthesized iron oxide nanoparticles would not show any particular structural shape (e.g., classical spherical nanoparticle morphology). The use of silk cocoons allows the preparation of iron oxide nanomaterials with more defined porosity and morphology with respect to classical methods.

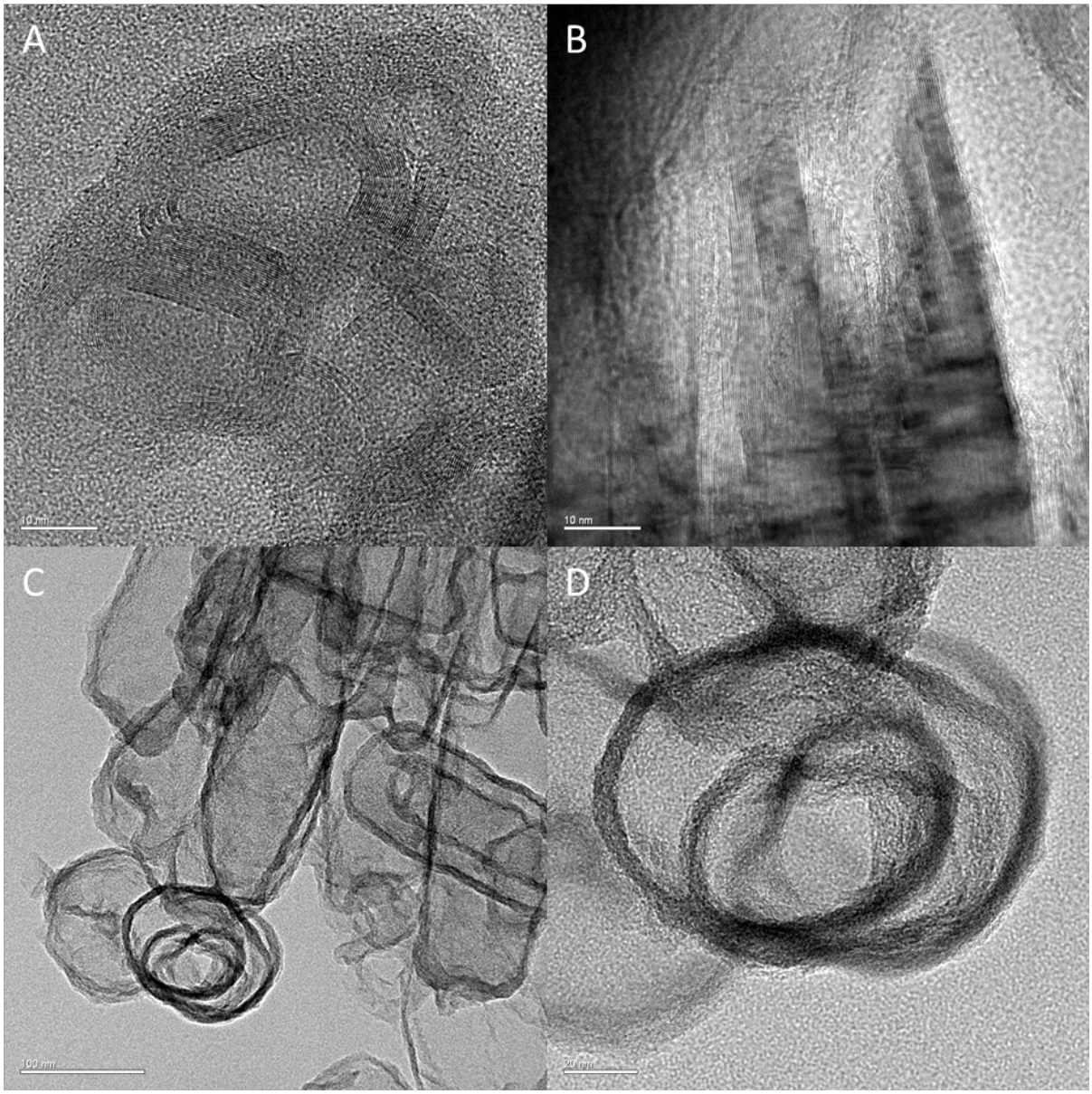

Figure 2. Transmission electron microscopy of samples calcined at (**A**): 100 °C, (**B**): 200 °C, and (**C**,**D**): 300 °C.

These samples were used in the microwave-assisted oxidation of benzyl alcohol. The obtained results are summarized in Table 1. First, almost negligible conversion (lower than 5%) was obtained in the absence of a catalyst, suggesting that the results presented in the table are due to the effect of the catalysts. All samples detected no products other than benzaldehyde and benzoic acid. Drying the sample for 48 h or 6 days leads to 14% and 10% conversion, respectively. The related selectivity in benzaldehyde is 96.6% and 97.1%. After calcination at 100 °C and 200 °C, the materials do not overcome the blank activity, showing the inefficiency of these catalysts. However, an interesting conversion of 35% with selectivity in benzaldehyde of 90.2% could be obtained after thermal treatment at 300 °C. These collected data seem to indicate that higher crystallinity is beneficial for reactivity.

Table 1. Benzyl alcohol oxidation using 50 mg of catalyst, 2 mL of acetonitrile, 0.2 mL of benzyl alcohol, 0.3 mL of H_2O_2 50%, CEM-Discover, 300 W, 200 °C, 240 PSI, 5 min.

Material	Conversion (%)	Selectivity Benzaldehyde (%)	Selectivity Benzoic Acid (%)
Blank	<5	100	0
Cocoon Fe-mag dried 48 h	14	96.6	3.4
Cocoon Fe-mag dried 6 days	10	97.1	2.9
Cocoon Fe-mag cal 100	<5	100	0
Cocoon Fe-mag cal 200	<5	100	0
Cocoon Fe-mag cal 300	35	90.2	9.8

The calcination temperature's impact on the material structure and reactivity showed thermal treatments at higher temperatures ranging from 500 °C to 800 °C. X-ray diffractograms as well as the reference of hematite alpha-Fe_2O_3 (PDF number 89-0597), are compiled in Figure 3. According to this XRD analysis, only hematite alpha-Fe_2O_3 is present in the samples calcined at 500, 600, and 800 °C. These diffractograms measured the crystallite size of 31 nm, 41.6 nm, and 54.9 nm for samples treated at 500, 600, and 800 °C, respectively. Increasing the calcination temperature up to 600 °C or 800 °C leads to larger crystallite sizes. These larger crystallites logically developed a smaller specific surface area. Using the QXRD technique, the ratio between the crystalline phase and the amorphous part of the materials was determined. The amount of amorphous phase decreased at increasing calcination temperatures due to the thermal stability of the alpha-Fe_2O_3 phase (hematite) with respect to amorphous iron oxide. From 18.31 wt% for the material calcined at 500 °C, the amorphous phase decreased as low as 13.83 wt% after calcination at 800 °C. Intermediate calcination at 600 °C leads to a quantity of amorphous phase of 17.64 wt%. Thus, an important part of each material was successfully synthesized as crystalline phases.

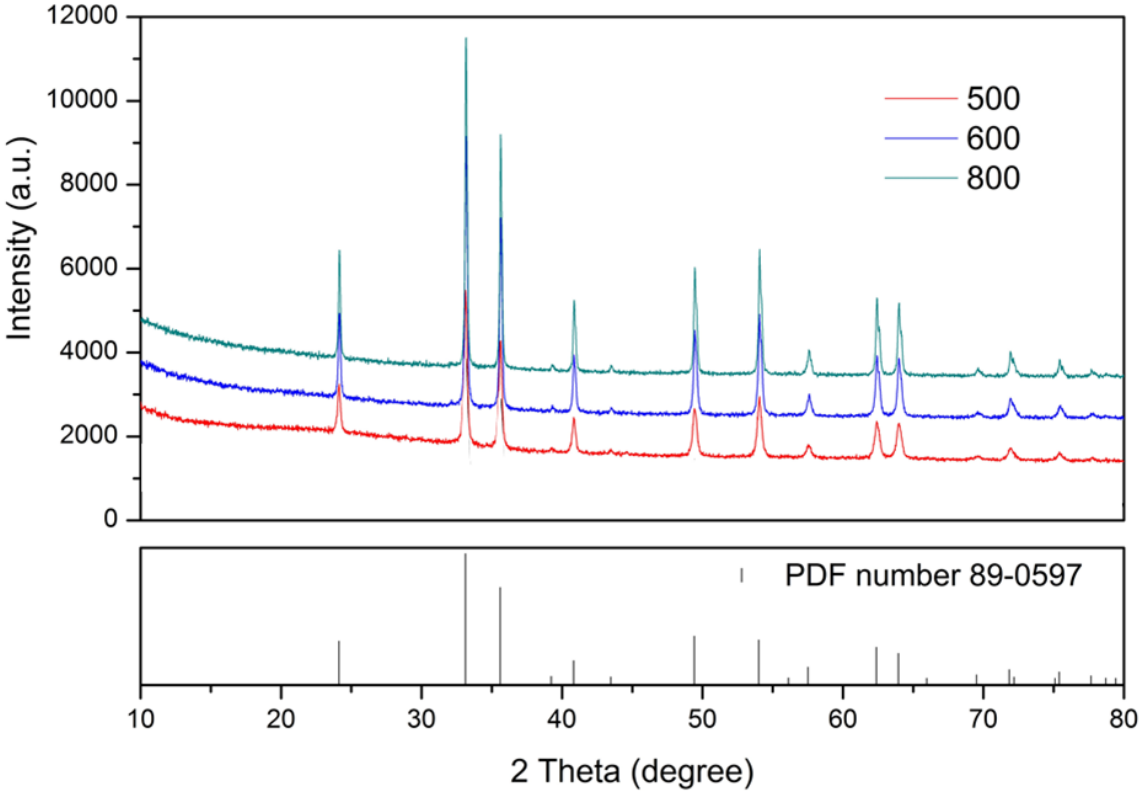

Figure 3. X-ray diffractograms of samples calcined at 500 °C, 600 °C, and 800 °C.

TEM images of the corresponding samples were compiled in Figure 4 with samples calcined at 500 °C, 600 °C, and 800 °C in Figure 4A, Figure 4B, and Figure 4C, respectively. Whatever the calcination temperature employed, a similar aspect with high homogeneity was observed. More precisely, the same type of porosity is detected, indicating the relative structural stability of the samples. Silk cocoon utilization is responsible for the defined porosity and morphology with respect to classical iron oxide synthesis methods. High-resolution transmission electron microscopy images of samples calcined at 500 °C, 600 °C, and 800 °C are presented in Figure 4D, Figure 4E, and Figure 4F, respectively. Similar periodic fringes were measured for the sample calcined at 500 °C and 800 °C with spaces of 0.3719 nm and 0.3659 nm, respectively. These values are consistent with the d-spacing corresponding to the (012) plane of alpha-Fe_2O_3, determined by SAED (Figure 4G,I). Concerning the material calcined at 600 °C, a periodic fringe of 0.2713 nm was measured. In this case, this spacing also corresponds to the d-spacing of the alpha-Fe_2O_3 but in the (104) plane (Figure 4H).

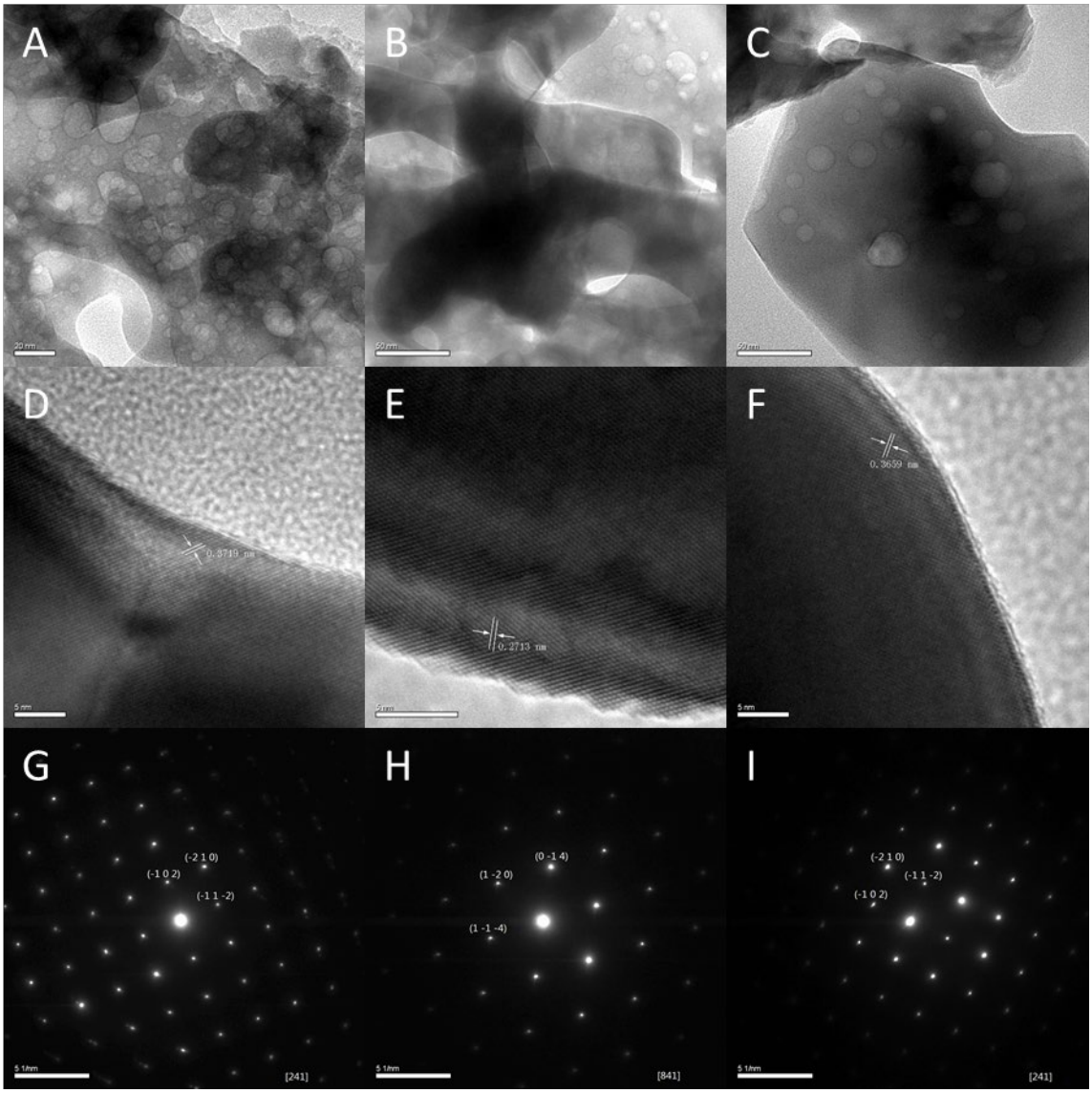

Figure 4. Transmission electron microscopy of samples calcined at (**A**): 500 °C, (**B**): 600 °C, and (**C**): 800 °C. High-resolution transmission electron microscopy of samples calcined at (**D**): 500 °C, (**E**): 600 °C, and (**F**): 800 °C. Selected area electron diffraction during high-resolution microscopy of samples calcined at (**G**): 500 °C, (**H**): 600 °C, and (**I**): 800 °C.

These materials were employed in the selective oxidation of benzyl alcohol to benzaldehyde. The obtained results are compiled in Table 2. As described in previous results, without a catalyst, a conversion lower than 5% is obtained during the oxidation of benzyl alcohol. Thus, the higher conversion and obtained selectivity are related to their catalytic effect. For all catalytic tests reported herein, only benzaldehyde and benzoic acid were detected as products of the reaction. During their first use, the conversion obtained with the different materials decreased as the calcination temperature increased. More precisely, conversions of 47%, 31%, and 12% were measured for the samples calcined at 500 °C, 600 °C, and 800 °C, respectively. The lower conversion obtained while increasing the temperature of calcination could be ascribed to the larger crystallites correlating with a smaller specific surface area of the iron oxide active phase. The related selectivity in benzaldehyde is 75.9%, 83.6%, and 94.6%. As expected, the selectivity in benzaldehyde increases as the conversion of benzyl alcohol decreases. Comparing these results with those previously reported in Table 1, an opposite trend is present with respect to the calcination temperature. Plotting the conversion with respect to calcination temperature leads to the visualization of a volcano-like curve, suggesting that an intermediate calcination temperature of 500 °C is favorable for the reaction. These trends can be explained by the following. On the one hand, increasing the calcination temperature decreases the amorphous phase in aid of the crystalline phase, suggesting it to be more active. In particular, the alpha-Fe_2O_3 phase (hematite) seems to be the active phase for the reaction. On the other hand, a calcination temperature too important could destabilize the active site leading to lower catalytic activity. Thus, the sample calcined at 500 °C benefits from the two-exposed contributions.

In order to test the stability of these three materials, recyclability tests were performed during four cycles. Unfortunately, the three materials are poorly recyclable. Taking as an example the Cocoon Fe-mag cal 500, while the conversion of benzyl alcohol decreased from 47% to 30%, 17%, and 16%, the selectivity in benzaldehyde increased from 75.9% to 90%, 92.1%, and 95.5% during the first, second, third, and fourth cycle, respectively. Once again, and as expected, the selectivity in benzaldehyde was higher for the lower conversion. Similar results were observed using different materials.

Table 2. Benzyl alcohol oxidation using 50 mg of catalyst, 2 mL of acetonitrile, 0.2 mL of benzyl alcohol, 0.3 mL of H_2O_2 50%, CEM-Discover, 300 W, 200 °C, 240 PSI, 5 min.

Material	Cycle	Conversion (%)	Selectivity Benzaldehyde (%)	Selectivity Benzoic Acid (%)
Blanco	-	<5	100	0
Cocoon Fe-mag cal 500	1	47	75.9	24.1
	2	30	90.0	10.0
	3	17	92.1	7.9
	4	16	95.5	4.5
Cocoon Fe-mag cal 600	1	31	83.6	16.4
	2	11	95.4	4,6
	3	15	97.2	2.8
	4	10	97.4	2.6
Cocoon Fe-mag cal 800	1	12	94.6	5.4
	2	<10	97.7	2.3
	3	<10	98.2	1.8
	4	<10	98.2	1.8

3. Experimental Section

3.1. Material Preparation

Silk cocoons (5 g) were crushed and ground in a ball mill (Retsch, PM 100) at 300 rpm for 20 min with the appropriate quantity of metal precursor ($FeCl_3.6H_2O$) to reach a theoretical 5 wt.% iron loading in the material. Samples were then collected and calcined under Nitrogen atmosphere (50 mL/min) at different temperatures, namely 100, 200, 300, 500, 600 and 800 °C, respectively. All materials with the exception of samples calcined at 500 °C and higher temperatures (see results and discussion for iron oxide phases present in these materials).

3.2. Characterization Techniques

X-ray powder diffraction data were collected using a D8 Advanced Diffractometer (Bruker AXS) with a Lynxeye detector, which operated at 40 kV and 40 mA with Cu Kα radiation at room temperature. The 2θ scan range was from 10° to 90°, with a step size of 0.02° and a counting time of 0.2 s for phase identification and 0.5 s for phase quantification. Phase identifications were conducted using the Bruker Diffrac-plus EVA software, supported by the Powder Diffraction File (PDF) database of the International Centre for Diffraction Data (ICDD). Crystallite size was determined by the Scherrer equation using the most intense peak to obtain precise results. Quantitative X-ray diffraction (QXRD) analysis was carried out with TOPAS 4.2 software (Bruker AXS GmbH, Germany). All of the samples were mixed with 45 wt% of CaF_2 (449717-25G, Merck, Germany) as the internal standard in our QXRD technique to assist in quantifying the amorphous content.

The morphologies of different materials were examined by transmission electron microscopy (TEM), high-resolution TEM (HRTEM), and selected-area electron diffraction (SAED) using an FEI Tecnai G2 20 S-TWIN Scanning Transmission Electron Microscope System and a JEOL 2010F transmission electron microscope.

3.3. Catalytic Activity

The catalytic activity of the prepared materials was tested in the oxidation reaction of benzyl alcohol. In total, 50 mg of catalyst was added to the reaction solution containing 2 mL of acetonitrile, 0.2 mL of benzyl alcohol, and 0.3 mL of H_2O_2 50%. The reaction was conducted with a CEM-discover microwave reactor. A power of 300 W was applied, leading to a temperature of 200 °C for 5 min, with an auto-generated pressure of 240 PSI.

4. Conclusions

Nanostructured iron-based catalysts have been synthesized from the mechanochemical incorporation of iron precursors on silk cocoons as a sacrificial template. Designed catalysts have been proven to be promising materials for the oxidation of benzyl alcohol. X-ray diffraction studies pointed to the alpha-Fe_2O_3 (hematite) crystalline phase as an active phase for the reaction. An optimum in the temperature of calcination was determined around 500 °C. This phenomenon was ascribed to a higher crystallinity after treatment at elevated temperatures. A further temperature increase led to reduced activities due to deteriorated nanostructures (e.g., lower surface areas). The optimum Cocoon Fe-mag cal 500 reached a conversion of 47% with selectivity in benzaldehyde of 75.9%, benzoic acid being the only side product of the reaction.

Author Contributions: Conceptualization, R.L. and R.A.D.A.; Writing-original draft, T.L., R.A.D.A. and Z.A.A.O.; Investigation R.A.D.A. and Z.A.A.O., Writing-review and editing, T.L., R.L. and K.S.; Supervision, R.L. and L.V.; Funding acquisition, R.L. All authors have read and agreed to the published version of the manuscript.

Funding: This work was supported by the Distinguished Scientist Fellowship Program (DSFP) at King Saud University, Riyadh, Saudi Arabia. This publication has been supported by the RUDN University Scientific Projects Grant System, project N° 025233-2-000.

Acknowledgments: This work was supported by the Distinguished Scientist Fellowship Program (DSFP) at King Saud University, Riyadh, Saudi Arabia. This publication has been supported by the RUDN University Scientific Projects Grant System, project Nº 025233-2-000.

Conflicts of Interest: The authors declare no conflict of interest.

References

1. Li, J.; Li, M.; Sun, H.; Ao, Z.; Wang, S.; Liu, S. Understanding of the Oxidation Behavior of Benzyl Alcohol by Peroxymonosulfate via Carbon Nanotubes Activation. *ACS Catal.* **2020**, *10*, 3516–3525.
2. Necsoiu, I.; Balaban, A.T.; Pascaru, I.; Sliam, E.; Elian, M.; Nenitzescu, C.D. The mechanism of the etard reaction. *Tetrahedron* **1963**, *19*, 1133–1142.
3. Luo, J.; Yu, H.; Wang, H.; Wang, H.; Peng, F. Aerobic oxidation of benzyl alcohol to benzaldehyde catalyzed by carbon nanotubes without any promoter. *Chem. Eng. J.* **2014**, *240*, 434–442.
4. Patel, S.; Mishra, B.K. A novel lipopathic Cr (VI) oxidant for organic substrates: Kinetic study of oxidation of benzyl alcohol. *Int. J. Chem. Kinet.* **2006**, *38*, 651–656.
5. Kabilan, S.; Girija, R.; Reis, J.C.R.; Segurado, M.A.P.; de Oliveira, J.D.G. Oxidation of benzyl alcohol by pyridinium dichromate in acetonitrile. Using the para/meta ratio of substituent effects for mechanism elucidation. *J. Chem. Soc. Perkin Trans. 2* **2002**, *6*, 1151–1157.
6. Kotai, L.; Kazinczy, B.; Keszler, Á.; Holly, S.; Gács, I.; Banerji, K.K. Three Reagents In One: Ammonium Permanganate in the Oxidation of Benzyl Alcohol. *Z. FÜR Nat. B* **2001**, *56*, 823–825.
7. Jose, N.; Sengupta, S.; Basu, J.K. Selective production of benzaldehyde by permanganate oxidation of benzyl alcohol using 18-crown-6 as phase transfer catalyst. *J. Mol. Catal. A Chem.* **2009**, *309*, 153–158.
8. Pritchard, J.; Kesavan, L.; Piccinini, M.; He, Q.; Tiruvalam, R.; Dimitratos, N.; Lopez-Sanchez, J.A.; Carley, A.F.; Edwards, J.K.; Kiely, C.J.; et al. Direct Synthesis of Hydrogen Peroxide and Benzyl Alcohol Oxidation Using Au–Pd Catalysts Prepared by Sol Immobilization. *Langmuir* **2010**, *26*, 16568–16577.
9. Chaudhari, M.P.; Sawant, S.B. Kinetics of heterogeneous oxidation of benzyl alcohol with hydrogen peroxide. *Chem. Eng. J.* **2005**, *106*, 111–118.
10. ten Brink, G.-J.; Arends, I.W.C.E.; Sheldon, R.A. Green, Catalytic Oxidation of Alcohols in Water**.** *Science* **2000**, *287*, 1636–1639.
11. Steinhoff, B.A.; Fix, S.R.; Stahl, S.S. Mechanistic Study of Alcohol Oxidation by the $Pd(OAc)_2/O_2$/DMSO Catalyst System and Implications for the Development of Improved Aerobic Oxidation Catalysts. *J. Am. Chem. Soc.* **2002**, *124*, 766–767.
12. Bhalothia, D.; Tsai, D.-L.; Wang, S.-P.; Yan, C.; Chan, T.-S.; Wang, K.-W.; Chen, T.-Y.; Chen, P.-C. Ir-oxide mediated surface restructure and corresponding impacts on durability of bimetallic NiO_x@Pd nanocatalysts in oxygen reduction reaction. *J. Alloy Compd.* **2020**, *844*, 156160.
13. Bhalothia, D.; Chen, P.-C.; Yan, C.; Yeh, W.; Tsai, D.-L.; Chan, T.-S.; Wang, K.-W.; Chen, T.-Y. Heterogeneous assembly of Pt-clusters on hierarchically structured CoOx@$SnPd_2$@SnO_2 quaternary nanocatalysts manifesting oxygen reduction reaction performance. *New J. Chem.* **2020**, *44*, 9712–9724.
14. Bhalothia, D.; Hsiung, W.-H.; Yang, S.-S.; Yan, C.; Chen, P.-C.; Lin, T.-H.; Wu, S.-C.; Chen, P.-C.; Wang, K.-W.; Lin, M.-W.; et al. Submillisecond Laser Annealing Induced Surface and Subsurface Restructuring of Cu–Ni–Pd Trimetallic Nanocatalyst Promotes Thermal CO_2 Reduction. *ACS Appl. Energy Mater.* **2021**, *4*, 14043–14058.
15. Altaee, H.; Alshamsi, H.A. Selective oxidation of benzyl alcohol by reduced graphene oxide supported platinum nanoparticles. *J. Phys. Conf. Ser.* **2020**, *1664*, 012074.
16. Göksu, H.; Burhan, H.; Mustafov, S.D.; Şen, F. Oxidation of benzyl alcohol compounds in the presence of carbon hybrid supported platinum nanoparticles (Pt@CHs) in oxygen atmosphere. *Sci. Rep.* **2020**, *10*, 5439.
17. Nascimento, L.F.; Matsubara, E.Y.; Donate, P.M.; Rosolen, J.M. Catalytic behavior of ruthenium anchored on micronanostructured composite in selective benzyl alcohol oxidation. *Reac. Kinet. Mech. Cat.* **2013**, *110*, 471–483.
18. Yamaguchi, K.; Mizuno, N. Supported Ruthenium Catalyst for the Heterogeneous Oxidation of Alcohols with Molecular Oxygen. *Angew. Chem.* **2002**, *114*, 4720–4724.
19. Mandal, S.; Bando, K.K.; Santra, C.; Maity, S.; James, O.O.; Mehta, D.; Chowdhury, B. Sm-CeO_2 supported gold nanoparticle catalyst for benzyl alcohol oxidation using molecular O_2. *Appl. Catal. A Gen.* **2013**, *452*, 94–104.
20. Alhumaimess, M.; Lin, Z.; Weng, W.; Dimitratos, N.; Dummer, N.F.; Taylor, S.H.; Bartley, J.K.; Kiely, C.J.; Hutchings, G.J. Oxidation of Benzyl Alcohol by using Gold Nanoparticles Supported on Ceria Foam. *ChemSusChem* **2012**, *5*, 125–131.
21. Chan-Thaw, C.E.; Savara, A.; Villa, A. Selective benzyl alcohol oxidation over Pd catalysts. *Catalysts* **2018**, *8*, 431.
22. Li, G.; Enache, D.I.; Edwards, J.; Carley, A.F.; Knight, D.W.; Hutchings, G.J. Solvent-free oxidation of benzyl alcohol with oxygen using zeolite-supported Au and Au–Pd catalysts. *Catal. Lett.* **2006**, *110*, 7–13.
23. Enache, D.I.; Edwards, J.K.; Landon, P.; Solsona-Espriu, B.; Carley, A.F.; Herzing, A.A.; Watanabe, M.; Kiely, C.J.; Knight, D.W.; Hutchings, G.J. Solvent-Free Oxidation of Primary Alcohols to Aldehydes Using Au-Pd/TiO_2 Catalysts. *Science* **2006**, *311*, 362–365.

24. Dimitratos, N.; Villa, A.; Wang, D.; Porta, F.; Su, D.; Prati, L. Pd and Pt catalysts modified by alloying with Au in the selective oxidation of alcohols. *J. Catal.* **2006**, *244*, 113–121.
25. Element Scarcity—EuChemS Periodic Table. Available online: https://www.euchems.eu/euchems-periodic-table/ (accessed on 13 April 2020).
26. González-Arellano, C.; Campelo, J.M.; Macquarrie, D.J.; Marinas, J.M.; Romero, A.A.; Luque, R. Efficient microwave oxidation of alcohols using low-loaded supported metallic iron nanoparticles. *ChemSusChem* **2008**, *1*, 746–750.
27. Balu, A.M.; Pineda, A.; Yoshida, K.; Campelo, J.M.; Gai, P.L.; Luque, R.; Romero, A.A. Fe/Al synergy in Fe_2O_3 nanoparticles supported on porous aluminosilicate materials: Excelling activities in oxidation reactions. *Chem. Commun.* **2010**, *46*, 7825–7827.
28. Rajabi, F.; Karimi, N.; Saidi, M.R.; Primo, A.; Varma, R.S.; Luque, R. Unprecedented selective oxidation of styrene derivatives using a supported iron oxide nanocatalyst in aqueous medium. *Adv. Synth. Catal.* **2012**, *354*, 1707–1711.
29. Pineda, A.; Balu, A.M.; Campelo, J.M.; Romero, A.A.; Carmona, D.; Balas, F.; Santamaria, J.; Luque, R. A Dry Milling Approach for the Synthesis of Highly Active Nanoparticles Supported on Porous Materials. *ChemSusChem* **2011**, *4*, 1561–1565.
30. Rajabi, F.; Naserian, S.; Primo, A.; Luque, R. Efficient and Highly Selective Aqueous Oxidation of Sulfides to Sulfoxides at Room Temperature Catalysed by Supported Iron Oxide Nanoparticles on SBA-15. *Adv. Synth. Catal.* **2011**, *353*, 2060–2066.
31. Balu, A.M.; Lin, C.S.K.; Liu, H.; Li, Y.; Vargas, C.; Luque, R. Iron oxide functionalised MIL-101 materials in aqueous phase selective oxidations. *Appl. Catal. A Gen.* **2013**, *455*, 261–266.
32. Xiao, S.; Zhang, C.; Chen, R.; Chen, F. Selective oxidation of benzyl alcohol to benzaldehyde with H_2O_2 in water on epichlorohydrin-modified Fe_3O_4 microspheres. *New J. Chem.* **2015**, *39*, 4924–4932.
33. Which Country Produces the Most Silkworm Cocoons? Available online: https://www.helgilibrary.com/charts/which-country-produces-the-most-silkworm-cocoons (accessed on 2 September 2022).